PHYSICAL REVIEW B **83**, 121409(R) (2011)

Detection of defects buried in metallic samples by scanning microwave microscopy

C. Plassard,[1] E. Bourillot,[1] J. Rossignol,[1] Y. Lacroute,[1] E. Lepleux,[2] L. Pacheco,[2] and E. Lesniewska[1]
[1]*Institut Carnot de Bourgogne, UMR CNRS 5209, CNRS-Université de Bourgogne, F-21078 Dijon Cedex, France*
[2]*ScienTec, F-91952 Les Ulis, France*

(Received 16 February 2011; published 28 March 2011)

This paper reports the local detection of buried calibrated metal defects in metal samples by a new experimental technique, scanning microwave microscopy. This technique combines the electromagnetic measurement capabilities of a microwave vector network analyzer with the subnanometer-resolution capabilities of an atomic force microscope. The network analyzer authorizes the use of several frequencies in the range 1–6 GHz, allowing three-dimensional tomographical investigation, which is useful for the detection of bulk defects in metal materials.

DOI: 10.1103/PhysRevB.83.121409 PACS number(s): 78.70.Gq, 07.79.Lh, 81.05.Ni, 81.70.Tx

Measuring electromagnetic properties of materials can provide insight into applications in many areas of science; increasingly, these properties need to be evaluated at the nanometer scale. Electromagnetic properties are ultimately related to a material's molecular structure and correlated to the detailed physical structure of a material with its electromagnetic properties. The nondestructive control of submicronic defects is, at the current time, crucial to the metals industry, and is bound to influence the distribution of defects in this scale, subsequently affecting the damage in the macroscopic scale. Currently, only destructive techniques, such as secondary-ion mass spectroscopy (SIMS), allow the characterization of such defects.

Since the invention of scanning tunneling microscopy (STM)[1] and the development of atomic force microscopy (AFM)[2] and related techniques such as lateral force microscopy (LFM),[3] the characterization of surface properties of various samples from materials to biological specimens has been achieved. All these microscopy techniques provide information about the surface, however, industrial applications require the investigation of the volume of samples. By analogy with the electromagnetism and with the development of scanning near-field optical microscopy (SNOM),[4–6] the bulk properties were interfering with image formation.

Already existing experimental techniques such as acoustic or ultrasonic microscopy[7] and scanning thermal microscopy (SThM)[8,9] provide information about defects in the volume. In fact, the matrix is generally a dielectric material that includes metal defects. These techniques are not usable for samples that are entirely metal.

Recently, in 2008, Agilent Technologies developed a new scanning probe microscopy (SPM) technique that combines the electromagnetic measurement capabilities of a microwave vector network analyzer (VNA N5230A, Agilent Technologies) with the nanometer resolution and angstrom-scale-positioning capabilities of an atomic force microscope (AFM 5600LS, Agilent Technologies); this new technique is scanning microwave microscopy (SMM). This nondestructive technique allows the characterization of defects located in the volume of a metal sample. Moreover, contrary to other experimental techniques such as scanning thermal microscopy, ultrasonic microscopy, etc., the sample does not undergo any form of constraint, e.g., mechanical or thermal, or of external circuitry allowing the differentiation of the behavior of materials. This new experimental technique was used for a tomographic study on a calibrated metal sample having buried metal defects in the sample in order to observe the effect of various frequencies on the investigation depth.

The principle of operation of SMM is the following: A microwave signal is sent directly from the network analyzer and transmitted through a resonant circuit to a conductive AFM probe that is in contact with a sample being scanned. The connection between the network analyzer and the tip is carried out using a coaxial cable. The cantilever and the probe act as a local radiant antenna for emission and reception of the electromagnetic field.[10] By analogy with an optic technique such as SNOM,[11] and like many SPM techniques,[12] the transmitter-receiver system is limited to interaction between the tip and the surface sample and makes it possible to capture the reflected microwave signal from the contact point.

By directly measuring the complex reflection coefficient from the network analyzer, the impedance representing the probe-sample interaction—amplitude and phase—at each scanned point can then be recorded, simultaneously with the surface topography.

The spatial resolution of the SMM has been evaluated on calibrated samples by direct measurement of the capacitance to ground between an AFM tip and a sample at microwave frequencies in the range 1–6 GHz. We noticed that the SMM images are acquired in real space, as in photon scanning tunneling microscopy.[13–17]

The tips used are traditional AFM tips of silicon nitride, Si_3N_4, 3 μm in height, of pyramidal form, associated with triangular levers having a constant of stiffness ranging between 0.1 and 0.6 N m^{-1}, covered with a Pt conducting layer, 100 nm thick.

In order to evaluate the influence of microwave frequency on the depth of investigation by SMM, calibrated samples in width and depth were carried out by electron-beam lithography (EBL) by using a scanning electron microscope (SEM).

A thin layer of 300-nm-thick electrosensitive polymer, poly(methyl methacrylate) (PMMA), is deposited on the silicon surface. We insulate the electrosensitive resin point by point. A solvent combination makes it possible thereafter to dissolve the marked polymer areas revealing the desired patterns. Reactive ion etching was performed in order to reveal the design patterns, 30 nm deep.

The patterns in relief were filled with Al film, 20 nm thick. Then, a 95-nm-thick nickel layer was evaporated in order to cover these structures. We obtained buried structures of Al

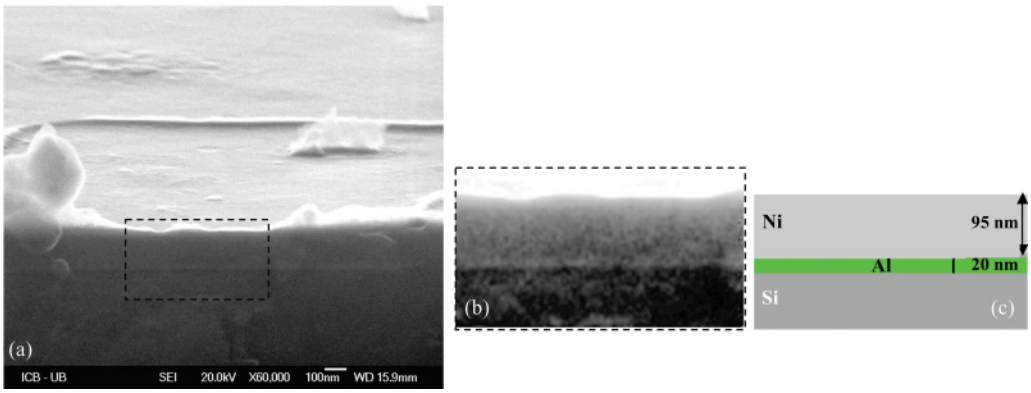

FIG. 1. (Color online) SEM images of L-shaped pattern with Al. (a) SEM image of a section of calibrated sample; (b) closeup of the L-shaped pattern with Al; (c) diagram of the calibrated sample.

under a calibrated layer of Ni whose cut after cleavage is presented in Fig. 1.

AFM observations at this final step have shown the same profile for the patterns, preserving a height difference of 10 nm (Fig. 2). On the topographic image [Fig. 2(a)], the outline of the patterns appears with a more important contrast. Traces of PMMA partially dissolved by the solvents remain present after evaporation of the layer of nickel. It was very difficult to obtain samples without topographical effects on the surface. We will use these residual traces later as reference marks for the investigation of the volume of the sample.

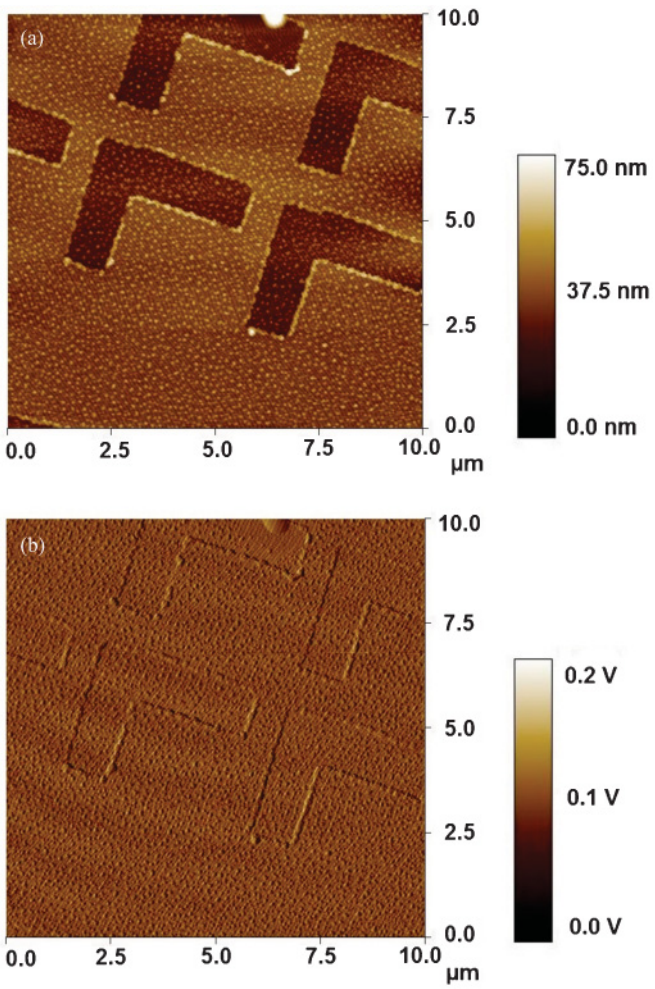

FIG. 2. (Color online) AFM images of calibrated sample: (a) topography; (b) friction.

Nevertheless, to show that the surface is composed of only one material, nickel, it is possible to use lateral force microscopy. While performing a scan at 90° compared to the direction of normal scanning, the cantilever will undergo torsions (lateral movements). These phenomena, more commonly called friction, highlight the differences of materials present at the surface of the sample.[18] An image of friction was carried out on this sample: In Fig. 2(b), it appears clearly that the substrate and the patterns are of the same nature—nickel only—as the color contrast is identical on the scale bar.

The calibrated metal samples were studied by SMM at different frequencies. Knowing the electromagnetic properties of nickel, i.e., $\mu_{r\mathrm{Ni}} = 600$, $\sigma_{\mathrm{Ni}} = 14.3 \times 10^6$ S m^{-1} at 20 °C, which constitutes the superior layer of the calibrated sample and considering that those properties remain constant in the frequency range used, it is possible to estimate, for each frequency, the depth of investigation by application of the *skin effect*.[19,20] Indeed, this physical phenomenon shows that the electromagnetic wave of high frequency has a weaker power of penetration in a metal sample than a wave of low frequency:

$$\delta = \frac{1}{\sqrt{\pi\,\mu_0\,\mu_r\,\sigma\,f}}, \tag{1}$$

with δ the skin thickness, μ_0 the magnetic permeability of vacuum ($4\pi \times 10^{-7}$), μ_r the permeability relating to the conductor, σ the electric conductivity in S m^{-1}, and f the frequency in Hz.

Thus, the potential of the microwave microscope lies in the possibility to differentiate the microwave images obtained at different frequencies and to allow the establishment of an in-depth cartography (Fig. 3). The microwave images presented in this figure provide information about the differences in phase, directly related to the nature of the material, obtained at various frequencies. The frequencies used to characterize the calibrated sample, as well as the corresponding depth, are specified in Fig. 3.

Before interpreting these results, it is advisable to recall that these experiments are subject to the theory on the

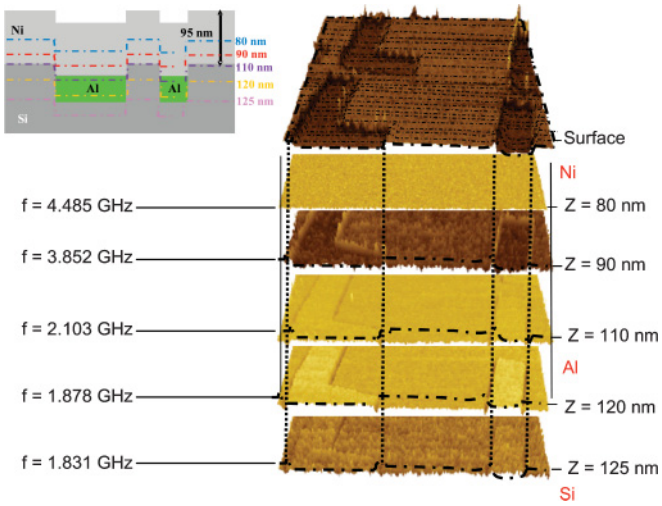

FIG. 3. (Color online) Three-dimensional tomographic image of the metal sample according to the frequency.

electromagnetic waves. Indeed, the expression of the wave reflected through a conductor is written

$$E_r = E_{r0}e^{\{j[\omega t-(z/\delta)]-(z/\delta)\}} = E_{r0}e^{j\omega t-(z/\delta)}e^{-j(z/\delta)}$$
$$= E_{r0}e^{j\omega t-(z/\delta)}e^{-j\phi} = E_{r0}e^{-z/\delta}e^{-j\phi}e^{j\omega t}, \quad (2)$$

with E_r the reflected electric field, E_{r0} the attenuated reflected electric field, ω the pulsation ($\omega = 2\pi f$), t the moment considered, z the component of the direction of propagation, and δ the penetration depth. The phase φ is defined by the expression

$$\varphi = \frac{z}{\delta}. \quad (3)$$

With a frequency of 4.485 GHz corresponding to an investigation depth of 80 nm, the scanned plane is located in the layer of nickel. The SMM image does not show any difference of phase at this depth; we are in the presence of a single and homogeneous material (nickel).

With a frequency of 3.852 GHz corresponding to an investigation depth of 90 nm, the scanned plane is located just at the top of Al patterns, in the bottom of the layer of nickel. The principal effect at this depth is related to the outline of the patterns. This outline appears much more clearly with phase contrast. This observation highlights a difference in the nature of the material since it is composed of PMMA resin whose physical properties differ completely from those of conductive materials.

With a frequency of 2.103 GHz corresponding to an investigation depth of 110 nm, the scanned plane is located in the upper part of the Al patterns and in the transition between the Si substrate and the Ni layer. The SMM image still reveals a light dephasing between the interior of the Al patterns (more clearly) and the Ni layer, thus marking a difference between the electromagnetic properties of two conductive metals, $\mu_{r\mathrm{Al}} = 1$, $\sigma_{\mathrm{Al}} = 3.5 \times 10^7$ S m^{-1} at 20 °C. An inversion of contrast is also remarkable compared to the preceding case, and can be explained by the fact that in this case the SMM image translates the answer of the reflected signal resulting from two conductive materials, Al and Ni.

With a frequency of 1.878 GHz corresponding to an investigation depth of 120 nm, the scanned plane is located inside the Al patterns. The SMM image clearly shows an important dephasing between the interior of the patterns (Al) and the Si substrate. Indeed, the Si substrate is of dielectric nature and does not present electromagnetic properties comparable with those of conductive materials, $\mu_{r\mathrm{Si}} \sim 1$, $\sigma_{\mathrm{Si}} = 1.2 \times 10^{-3}$ S m^{-1} at 20 °C. By using Eq. (3) again, it is possible to express the dephasing introduced by each material, for a frequency f and the same component z:

For the Al structures, $\phi_{\mathrm{Al}} = \frac{z}{\delta_{\mathrm{Al}}}$, where $\delta_{\mathrm{Al}} = \frac{1}{\sqrt{\pi\,\mu_0\,\mu_{\mathrm{Al}}\,\sigma_{\mathrm{Al}}\,f}}$.

For the Si substrate, $\phi_{\mathrm{Si}} = \frac{z}{\delta_{\mathrm{Si}}}$, where $\delta_{\mathrm{Si}} = \frac{1}{\sqrt{\pi\,\mu_0\,\mu_{\mathrm{Si}}\,\sigma_{\mathrm{Si}}\,f}}$.

Thus, for the same frequency f, we have $\delta_{\mathrm{Al}} < \delta_{\mathrm{Si}}$ because $\mu_{\mathrm{Al}}\sigma_{\mathrm{Al}} > \mu_{\mathrm{Si}}\sigma_{\mathrm{Si}}$.

On the level of dephasing, $\phi_{\mathrm{Al}} > \phi_{\mathrm{Si}}$. The dephasing introduced by the Al structures is thus more important than that of the Si substrate, thus justifying the phase contrast observed on the SMM image.

With a frequency of 1.831 GHz corresponding to an investigation depth of 125 nm, the scanned plane is located just below the Al patterns, in the Si substrate. On the SMM image, there is no difference of phase between the interior of the patterns and the Si substrate. This means that the SMM image represents only the Si substrate. The outline of the patterns is observable, showing once again that the PMMA resin has a chemical nature and physical properties different from those of Si.

Another important parameter of SMM lies in its lateral resolution. This resolution is closely related to the coupling of

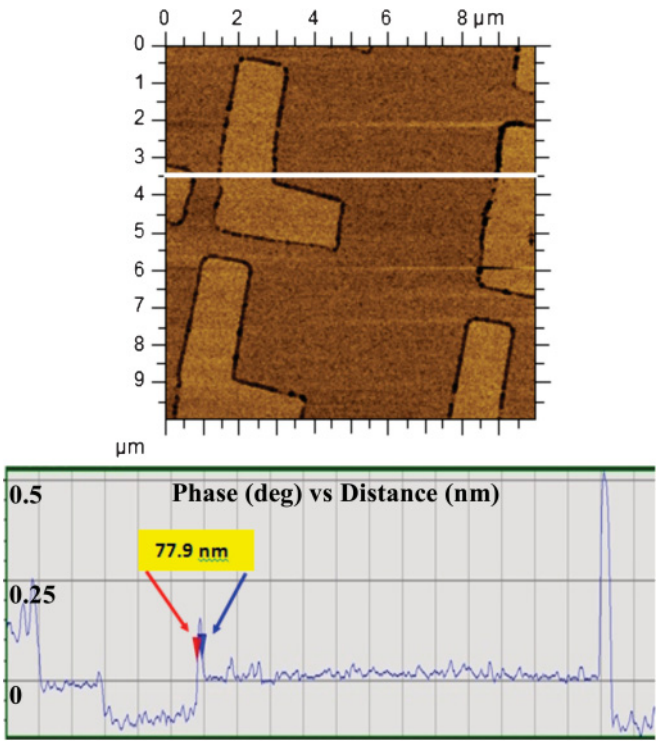

FIG. 4. (Color online) Estimation of the SMM resolution on phase image at $f = 1.878$ GHz.

the electromagnetic wave in the end of the tip and the sample. It is obvious that when the tip is damaged, the resolution of the apparatus is degraded immediately, as with other experimental techniques, such as SNOM.[11]

The resolution of the microscope could be estimated while measuring, directly on the microwave images, the width of the outline of the Al patterns. A profile was carried out on the phase image of 10-μm range (Fig. 4), placing the two cursors at the middle height of the peak, representing the outline of the pattern. The result shows a resolution $<$80 nm, knowing that it can still be improved for recorded images with a smaller buried calibrated sample.

In conclusion, the series of experiments showed the capacity of SMM microscopy to detect defects located in the volume of a metal sample. It more precisely makes it possible to directly relate the investigation depth associated to the frequency used. Moreover, the repetition of measurements at several different frequencies gives access to a tomographic study of the sample. Its resolution allows the mapping of the nanometric defect, $<$80 nm in depth.

This study proves the capacity of the scanning microwave microscope to detect defects in the volume of a purely metal sample. Moreover, contrary to the other experimental techniques investigating the volume of a sample, this one has the advantage of being completely nondestructive.

The investigation of in-depth defects in metal alloys is thus made possible. Defects of micrometric depth could be characterized by using weaker frequencies (improvement of the resonant circuit). This apparatus has great potential for use in many fields in the metallurgical industry, e.g., alloys, stainless steel, etc.

We acknowledge the financial support of the technical center of AREVA NP (Le Creusot, France), the management of Welience, and the nuclear consortium Pole Nucleaire de Bourgogne (Dijon, France).

[1]G. Binnig, H. Rohrer, C. Gerber, and E. Weibel, Phys. Rev. Lett. **49**, 57 (1982).

[2]G. Binnig, C. F. Quate, and C. Gerber, Phys. Rev. Lett. **56**, 930 (1986).

[3]G. Meyer and N. M. Amer, Appl. Phys. Lett. **57**, 2089 (1990).

[4]J. C. Weeber, E. Bourillot, A. Dereux, J. P. Goudonnet, Y. Chen, and C. Girard, Phys. Rev. Lett. **77**, 5332 (1996).

[5]J. R. Krenn, A. Dereux, J. C. Weeber, E. Bourillot, Y. Lacroute, J. P. Goudonnet, G. Schider, W. Gotschy, A. Leitner, F. R. Aussenegg, and C. Girard, Phys. Rev. Lett. **82**, 2590 (1999).

[6]J. R. Krenn, J. C. Weeber, A. Dereux, E. Bourillot, J. P. Goudonnet, G. Schider, A. Leitner, F. R. Aussenegg, and C. Girard, Phys. Rev. B **60**, 5029 (1999).

[7]L. W. Kessler, in *ASM Handbook Volume 17: Nondestructive Evaluation and Quality Control* (ASM International, Metals Park, OH, 1989), p. 465.

[8]G. Mills, J. M. R. Weaver, G. Harris, W. Chen, J. Carrejo, L. Jonhson, and B. Rogers, Ultramicroscopy **80**, 7 (1999).

[9]J. H. Lee and Y. B. Gianchandani, Rev. Sci. Instrum. **75**, 1222 (2009).

[10]A. Kramer, F. Keilmann, B. Knoll, and R. Guckenberger, Micron **27**, 413 (1996).

[11]C. Chicanne, T. David, R. Quidant, J. C. Weeber, Y. Lacroute, E. Bourillot, A. Dereux, G. Colas des Francs, and C. Girard, Phys. Rev. Lett. **88**, 097402 (2002).

[12]W. S. Chang, S. Bauerdick, and M. S. Jeong, Ultramicroscopy **108**, 1070 (2008).

[13]E. Bourillot, F. De Fornel, J. P. Goudonnet, D. Persegol, A. Kevorkian, and D. Delacourt, J. Opt. Soc. Am. A **12**, 95 (1995).

[14]J. P. Goudonnet, E. Bourillot, P. M. Adam, F. De Fornel, L. Salomon, P. Vincent, M. Neviere, and T. L. Ferrell, J. Opt. Soc. Am. A **12**, 1749 (1995).

[15]E. Bourillot, S. I. Hosain, J. P. Goudonnet, G. Voirin, and G. Kotrotsios, Phys. Rev. B **51**, 11225 (1995).

[16]N. Richard, A. Dereux, T. David, E. Bourillot, J. P. Goudonnet, F. Scheurer, E. Beaurepaire, and G. Garreau, Phys. Rev. B **59**, 5936 (1999).

[17]E. Devaux, A. Dereux, E. Bourillot, J. C. Weeber, Y. Lacroute, J. P. Goudonnet, and C. Girard, Phys. Rev. B **62**, 10504 (2000).

[18]A. J. Den Boef, Rev. Sci. Instrum. **62**, 88 (2009).

[19]G. Bekefi and A. H. Barrett, *Electromagnetic Vibrations, Waves and Radiation* (MIT Press, Cambridge, MA, 1977).

[20]V. Belevitch, Philips Tech. Rev. **32**, 221 (1971).